Science Advances

AAAS

advances.sciencemag.org/cgi/content/full/4/3/eaap7314/DC1

Supplementary Materials for

Temperature effect on phase state and reactivity controls atmospheric multiphase chemistry and transport of PAHs

Qing Mu, Manabu Shiraiwa, Mega Octaviani, Nan Ma, Aijun Ding, Hang Su, Gerhard Lammel, Ulrich Pöschl, Yafang Cheng

Published 21 March 2018, *Sci. Adv.* **4**, eaap7314 (2018)
DOI: 10.1126/sciadv.aap7314

This PDF file includes:

- text S1. Problems without considering bulk processes.
- text S2. Warm conveyor belts (WCBs) and BaP transport in Gosan winter case.
- table S1. Flow tube experiments of multiphase degradation of BaP with ozone.
- table S2. Kinetic parameters used in the KM-SUB simulation for the ozonolysis of BaP to reproduce experiment results of the Zhou scheme.
- table S3. Parameterization of multiphase degradation rate for the ozonolysis of BaP.
- table S4. Comparisons of observed and predicted BaP concentrations in the regional WRF-Chem model and the global EMAC model.
- fig. S1. Same as Fig. 2B but with three more sensitivity studies.
- fig. S2. Multiphase degradation rate and chemical lifetime.
- fig. S3. BaP concentrations and multiphase degradation rate.
- fig. S4. Net meridional mass flux and vertical center of column mass for BaP in different cases.
- fig. S5. BaP transport due to WCB and frontal activities associated with mid-latitude cyclones for the Gosan winter case.
- fig. S6. A conceptual scheme for air pollution transport due to middle-latitude cyclone.
- References (*57–60*)

text S1. Problems without considering bulk processes.

The use of surface model without considering bulk diffusion/reaction results in a contradictory RH dependence of BaP degradation rates at different ozone concentrations. Taking the Zhou scheme for example, using such extrapolation resulted in a contradictory RH dependence of BaP degradation rates at different ozone ranges. The reactions of the Zhou scheme at 50 ppbv ozone were slower in 70% RH than 50% RH (Fig. 1A), contrary to their own conclusion that higher RH enhanced the reactivity of BaP.

text S2. Warm conveyor belts (WCBs) and BaP transport in Gosan winter case.

The frontal activities and WCBs associated with mid-latitude cyclones play a very important role in lifting plumes from the planetary boundary layer (PBL) to the free troposphere (FT), promoting long-range transport of air pollutants (*57*). Thus, such kind of transport processes can influence the chemical distributions of the middle- and upper- troposphere of downwind regions in Northeast Asia, the Pacific Ocean and even North America. In North China, transport processes due to WCBs have been found particularly frequent in summer resulting from the high frequency of mid-latitude cyclones, but they are also important in spring and winter. In order to understand the detailed transport mechanism for the high concentration of BaP in the middle troposphere of the Northern Hemisphere mid-latitudes, we chose a typical event during 25–26 February 2003 as case study.

Figure S5 shows that the Gosan outflow case in winter is a good example of PBL-FT transport. A mid-latitude cyclone (low pressure centered at 118° E, 43° N) was located in the north to North China Plain on early 25 Feb 2003 (fig. S5A). High moisture (represented by specific humidity) demonstrated a strong northeastward belt-shape transport from the boundary layer in the warm air frontal zone to the middle troposphere over the warm front, with clockwise shape belts overrunning the fronts (fig. S5C). Similarly, BaP showed a high concentration belt in front of the cold front (~ 850 hPa) and then got transported over the warm front (~700 hPa), hence, experienced fast eastward transport by westerlies (or jets) in the middle-troposphere (fig. S5B, 5D, 5F). A T-shape plume could be identified from the 700 hPa SH and BaP distributions over the warm front (fig. S5D). It includes a branch transported poleward in addition to the eastward branch. Ding et al. (*58*) reported a similar event in the same region and found that the WCB associated with the cyclone played the key role in lifting air pollutants from the boundary layer to the middle troposphere, and also pointed out that such kind of lifting provides the most important contribution for intercontinental and poleward transports in the Northern Hemisphere. To clearly demonstrate the structure of WCBs and other related flows in the cyclone, a conceptual model is given in fig. S6. Since cyclone is one of the most dominant synoptic features in the mid-latitudes, such kind of WCB-induced lifting could be the main contribution to high and long-range transported pollutants, like BaP.

table S1. Flow tube experiments of multiphase degradation of BaP with ozone. Langmuir-Hinshelwood first-order reaction rate coefficient $k = \frac{k_{max} k_{o3}[O_3]}{1+k_{o3}[O_3]}$. For Kahan scheme, $k = \frac{A*[O_3]}{B+[O_3]}$. $[O_3]$ is in molecules cm^{-3}.

Scheme	Substrate	Coating	O_3 (ppmv)	T (K)	RH (%)	k_{max} (s^{-1})	k_{O3} (10^{-15} cm^3)
Pöschl (*4*)	spark discharge soot	None	0.05–1	296 ±2	0	0.015±0.001	270±40
					25	0.016±0.001	280±20
Kwamena (*22*)	azelaic acid	None	2–45	298±5	0	0.048±0.008	1.2±0.4
					72	0.060±0.018	2.8±1.4
	NaCl				0	0.032	<0.12
Kahan (*5*)	octanol	None	15–950	room	0	A=(5.5±0.2)*$10^{-3}s^{-1}$	B=(2.8±0.4)*10^{15} molec cm^{-3}
Zhou (*6*)	ammonium sulfate	None	4–25	296 ± 3	<5%	0.034 ± 0.002	14 ± 4
		bis(2-ethylhexyl)sebacate	6–32			0.051 ± 0.001	4.1 ± 0.1
		phenylsiloxane oil	4–32			0.047 ± 0.004	13 ± 4
		eicosane	6–32			shut off	shut off
Zhou (*11*)	ammonium sulfate	a-pinene SOA 5─10 nm	1.5–16	296 ± 3	<5%	0.042 ± 0.004	5.1 ± 0.9
		a-pinene SOA 20─80 nm	8–24		<5%	0.022 ± 0.003	2.3 ± 0.4
			3–24		50%	0.023 ± 0.004	14 ± 4.4
			3–28		70%	0.039 ± 0.004	6.2 ± 1.1

table S2. Kinetic parameters used in the KM-SUB simulation for the ozonolysis of BaP to reproduce experiment results of the Zhou scheme.

Parameter	Description	Value
α_{s,O_3}	surface accommodation coefficient of O_3	1 *
τ_{d,O_3} (s)	Desorption lifetime of O_3	3.2 x 10^{-9} *
$E_{a,pc}$ (kJ mol^{-1})	Activation energy from physisorbed O_3 to ROI	42 *,†
$E_{a,ox}$ (kJ mol^{-1})	Activation energy from ROI to oxidized BaP	80 *,†
k_{BR} (cm^3 s^{-1})	Second-order bulk reaction rate coefficient between BaP and O_3	5 x 10^{-18} †
$K_{sol,cc}$ (mol cm^{-3} atm^{-1})	Henry's law coefficient of O_3	6 x 10^{-4} †

* ref (*23*); † ref (*11*)

table S3. Parameterization of multiphase degradation rate for the ozonolysis of BaP. First-order reaction rate coefficients k (s^{-1}) are given by the Hill equation $k = \text{base} + \frac{\text{max}-\text{base}}{1+(\frac{\text{xhalf}}{[O_3]})^{\text{rate}}}$ with $[O_3]$ in ppbv. The R^2 of these Hill equation fits are all larger than 0.99. For each grid cell, the parameters are read from the look-up table with temperature and relative humidity (RH) closest to the temperature and humidity of the grid cell. When equally close, the smaller parameter value is adopted.

70% RH				
Temperature (°C)	**base**	**max**	**rate**	**xhalf**
40	1.67e-4	1.29e-2	0.682	1.25e3
35	1.19e-4	1.29e-2	0.682	1.25e3
30	8.52e-5	9.02e-3	0.696	1.23e3
25	5.94e-5	6.33e-3	0.707	1.27e3
23	4.84e-5	5.14e-3	0.700	1.25e3
15	2.55e-5	2.72e-3	0.711	1.29e3
10	1.58e-5	1.68e-3	0.706	1.27e3
5	9.49e-6	1.00e-3	0.698	1.24e3
0	6.85e-6	5.64e-4	0.704	1.11e3
-5	5.31e-6	3.10e-4	0.713	1.01e3
-10	3.83e-6	1.48e-4	0.731	7.33e2
-15	8.93e-7	1.05e-4	0.580	1.88e3
-20	1.16e-6	2.58e-5	0.673	3.35e2

50% RH				
Temperature (°C)	**base**	**max**	**rate**	**xhalf**
40	1.65e-4	1.80e-2	0.672	1.21e3
35	1.16e-4	1.27e-2	0.678	1.24e3
30	8.24e-5	8.68e-3	0.688	1.22e3
25	5.44e-5	5.71e-3	0.688	1.21e3
23	2.64e-5	3.08e-3	0.618	7.97e2
15	2.20e-6	1.10e-3	0.544	5.83e2
10	7.84e-7	2.60e-4	0.559	7.50e1
5	-4.79e-7	7.19e-5	0.564	1.31e1
0	-7.02e-6	2.18e-5	0.464	1.05e0
-5	-4.06e-6	6.54e-6	0.459	1.24e-1
-10	-1.89e-6	2.02e-6	0.429	1.44e-2
-15	2.58e-7	7.22e-7	0.175	1.28e-1
-20	1.79e-7	2.60e-7	0.689	1.11e3

Dry				
Temperature (°C)	**base**	**max**	**rate**	**xhalf**
40	1.61e-4	1.74e-2	0.667	1.19e3
35	1.10e-4	1.19e-2	0.667	1.21e3
30	6.75e-5	7.31e-3	0.653	1.11e3
25	2.3e-5	3.10e-3	0.586	7.02e2
23	-1.90e-5	9.28e-4	0.446	1.59e2
15	-2.65e-5	3.09e-4	0.341	8.38e1
10	-4.28e-5	1.03e-4	0.191	4.41e0
5	-1.12e-5	3.49e-5	0.142	4.33e0

0	3.39e-6	1.03e-5	0.382	8.85e2
-5	1.37e-6	5.67e-6	0.780	2.96e3
-10	4.53e-7	1.57e-6	0.979	1.63e3
-15	1.44e-7	2.10e-6	0.924	1.39e4

table S4. Comparisons of observed and predicted BaP concentrations in the regional WRF-Chem model and the global EMAC model. (**A**) Observed and predicted BaP concentrations (ng m^{-3}) over the period 2007–2009*. (**B**) Mean bias (prediction - observation) (ng m^{-3}) and relative bias ((prediction - observation) / observation) of BaP for various types of sites in Fig. 2A.

(**A**)

	Alert, Canada	Spitsbergen, Norway	Pallas, Finland	All mid-latitude stations
No. months	34†	23†	19†	405†
Mean				
Observation	1.40E-03	4.08E-03	1.01E-02	1.41E-01
Kwamena	8.15E-07	6.92E-06	1.22E-03	5.75E-02
ROI-T	1.64E-05	5.48E-05	4.68E-03	7.98E-02
Kahan	6.25E-03	5.22E-03	5.33E-02	2.72E-01
Pöschl	1.61E-07	1.07E-06	1.25E-04	5.88E-03
Median				
Observation	4.78E-04	8.80E-04	2.84E-03	3.74E-02
Kwamena	7.41E-07	2.73E-06	1.18E-03	1.82E-02
ROI-T	1.35E-05	2.61E-05	3.84E-03	3.24E-02
Kahan	4.45E-04	1.28E-03	4.64E-02	3.34E-01
Pöschl	1.48E-07	6.05E-07	1.16E-04	3.07E-03
Geometric mean ‡				
Observation	6.70E-04	1.38E-03	3.62E-03	4.60E-02
Kwamena	7.79E-07	4.00E-06	1.19E-03	2.57E-02
ROI-T	1.19E-05	2.89E-05	3.98E-03	3.43E-02
Kahan	4.61E-04	1.68E-03	4.21E-02	3.43E-01
Pöschl	1.57E-07	8.13E-07	1.20E-04	2.26E-03
Root mean square error				
Kwamena	6.26E-03	7.78E-03	2.37E-02	2.79E-01
ROI-T	6.25E-03	7.77E-03	2.24E-02	2.72E-01
Kahan	5.98E-03	1.14E-02	6.17E-02	5.71E-01
Pöschl	6.26E-03	7.78E-03	2.41E-02	2.89E-01

*Although improved performances, the ROI-T scheme still tends to underestimate BaP in the Arctic (sites Alert and Spitsbergen), probably because current atmospheric models generally underestimate co-emitted black carbon in the Arctic due to missing sources (*59, 60*). Therefore, the actual inflow of BaP to the Arctic could be even stronger.

†Values below limit of quantitation (LOQ) are treated as 0. Number of data <LOQ is 21 for Alert, 8 for Spitsbergen, 1 for Pallas and 0 for all mid-latitude stations.

‡Geometric mean is used in the study.

(**B**)

	Xianghe	Gosan	Arctic	Mid-latitude
Kwamena	6.76E-1 (0.87)	-7.88E-3 (-0.39)	-5.99E-03 (-3.17)	-8.40E-02 (-1.83)
ROI-T	-1.44E-2 (-1.80E-2)	-1.36E-3 (-6.80E-2)	-4.82E-03 (-2.55)	-6.16E-02 (-1.34)
Kahan	1.22 (1.56)	1.38E-1 (6.90)	1.42E-02 (7.51)	3.35E-01 (7.28)
Pöschl	7.33E-3 (9.40E-3)	-1.80E-2 (-0.90)	-6.38E-03 (-3.38)	-1.36E-01 (-2.96)

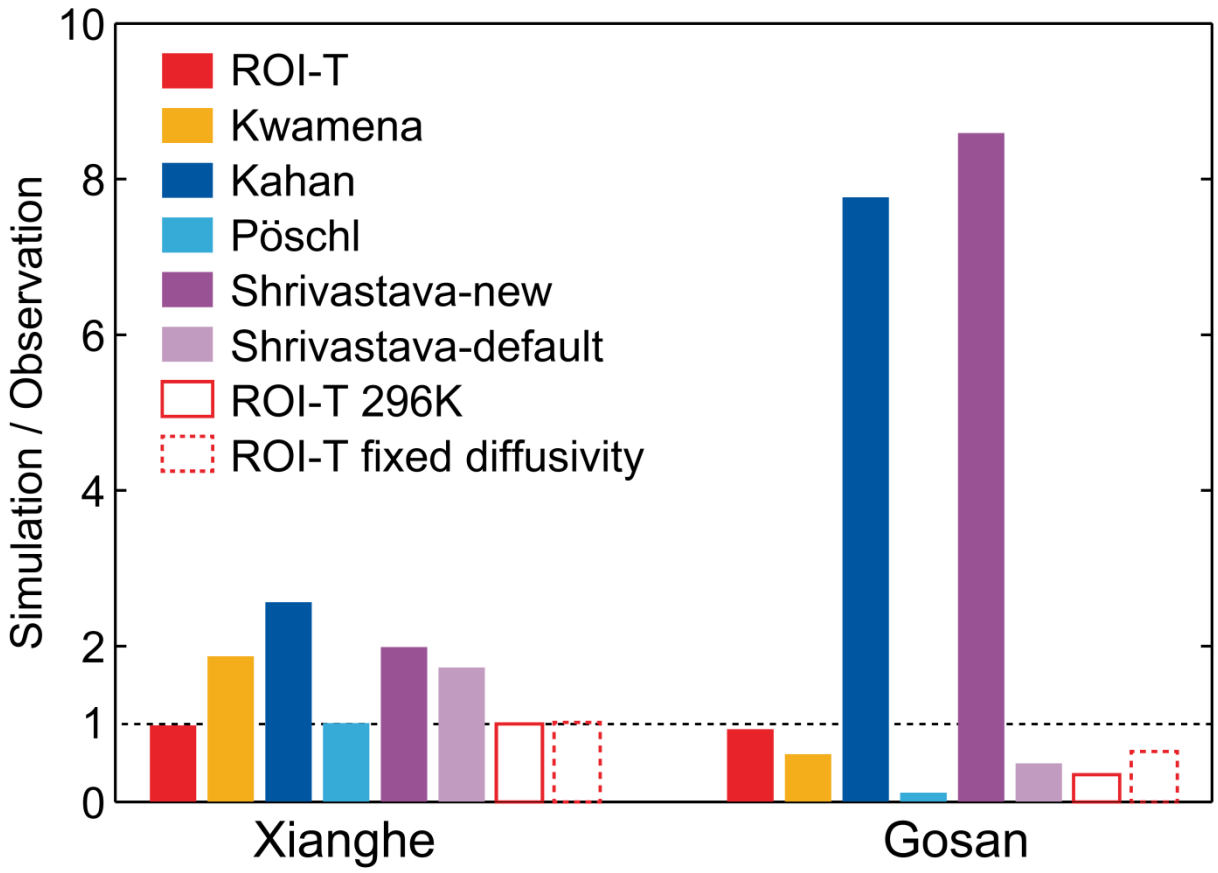

fig. S1. Same as Fig. 2B but with three more sensitivity studies. "Shrivastava-default" uses the default setting (the same as the thin coating case in the Zhou scheme (*11*)) in Shrivastava et al. (*14*) "ROI-T 296 K" fixes both OA diffusion coefficient and chemical reaction rate of BaP with ROI at 296 K level. "ROI-T fixed diffusivity" only fixes OA diffusion coefficient at 296 K level but allows the chemical reaction rate of BaP with ROI to change with temperature.

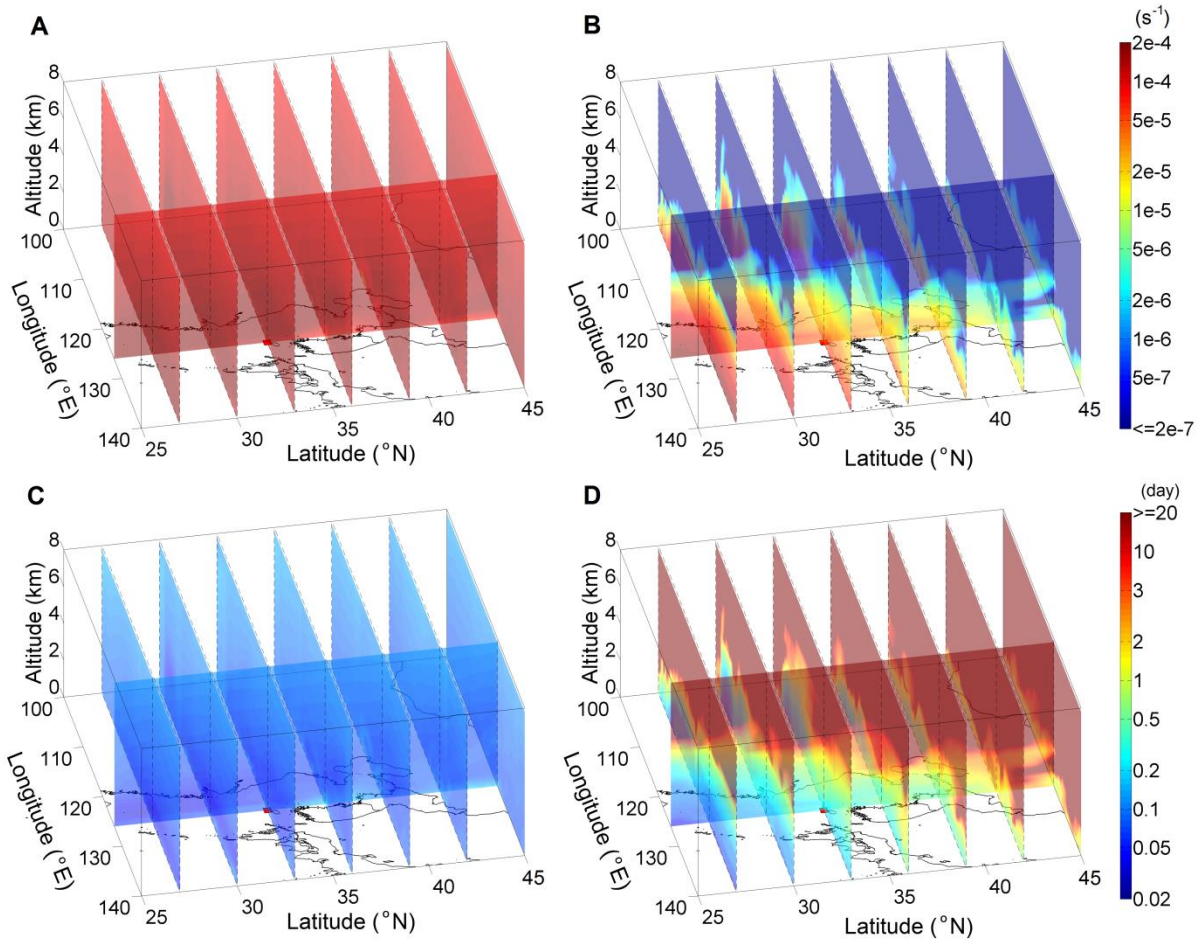

fig. S2. Multiphase degradation rate and chemical lifetime. Multiphase degradation rate *k* (s^{-1}, (**A**) for the Kwamena scheme, (**B**) for the ROI-T scheme) and chemical life time (day, (**C**) for the Kwamena scheme, (**D**) for the ROI-T scheme) on 24 February 2003 in the East Asia outflow case.

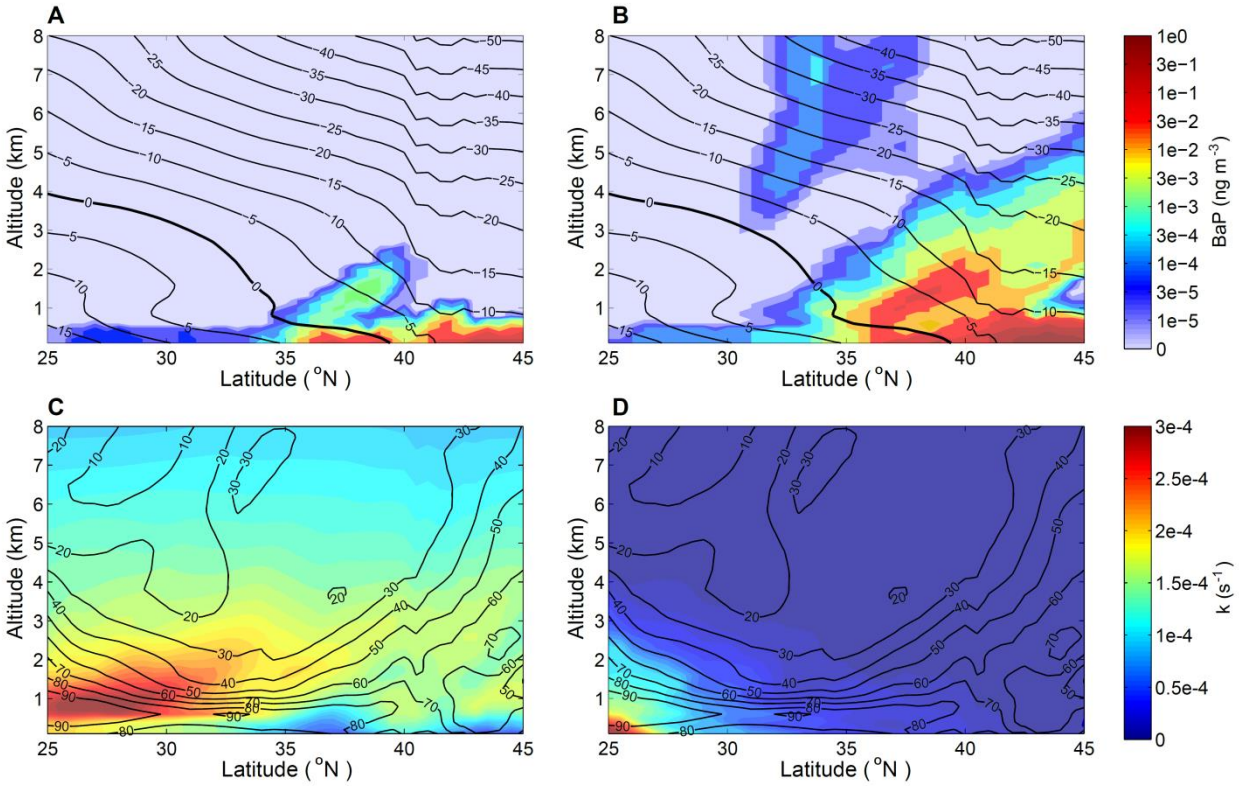

fig. S3. BaP concentrations and multiphase degradation rate. BaP concentrations (ng m^{-3}, (**A**) for the Kwamena scheme, (**B**) for the ROI-T scheme) and multiphase degradation rate *k* (s^{-1}, (**C**) for the Kwamena scheme, (**D**) for the ROI-T scheme) at a cross section of 126° E on 24 February 2003 in the East Asia outflow case. Temperature (ºC) contours are shown in A and B. RH (%) contours are shown in C and D.

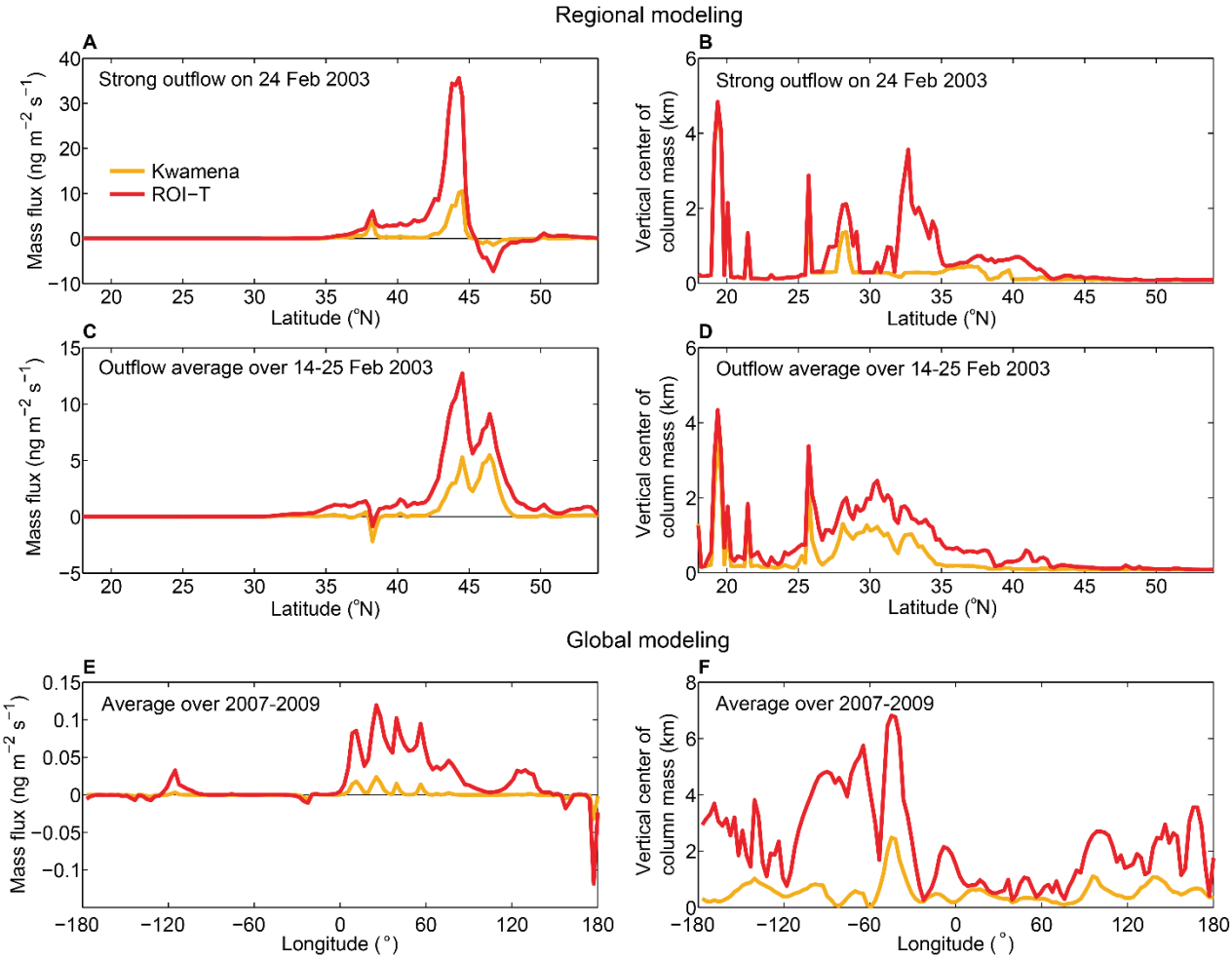

fig. S4. Net meridional mass flux and vertical center of column mass for BaP in different cases. (**A**) BaP mass fluxes and (**B**) vertical center of column mass at 126°E averaged during the East Asia outflow episode 24 February 2003. (**C**) BaP mass fluxes and (**D**) vertical center of column mass at 126°E averaged over simulation period 14–25 February 2003. (**E**) BaP mass fluxes and (**F**) vertical center of column mass across 65°N averaged over the years 2007–2009.

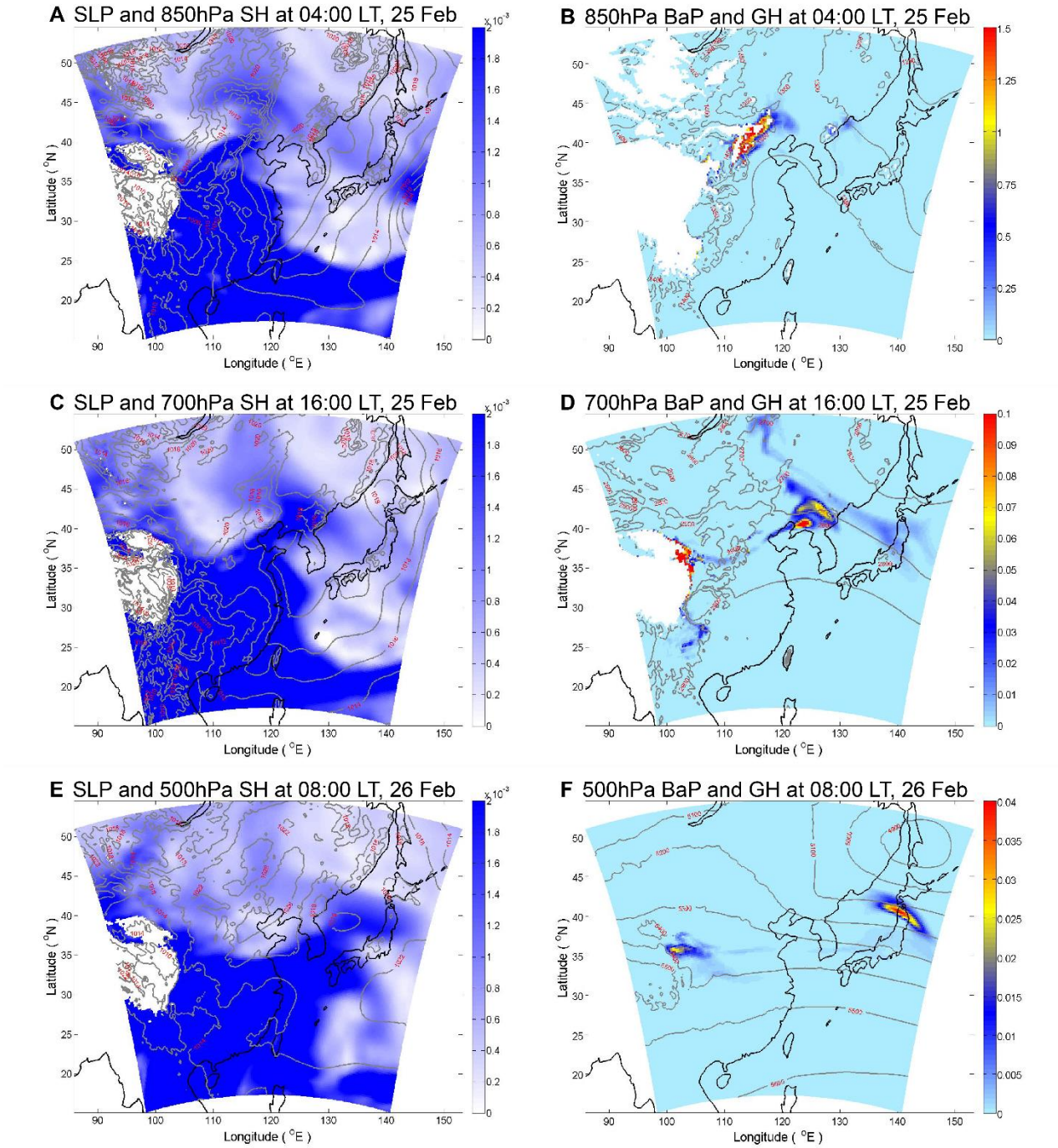

fig. S5. BaP transport due to WCB and frontal activities associated with mid-latitude cyclones for the Gosan winter case. The left column shows specific humidity (SH, g g^{-1}) and sea level pressure (SLP, hPa, contour lines) at different pressure level (**A**) 850 hPa, (**C**) 700 hPa, and (**E**) 500 hPa for a cyclone in East Asia during 25–26 February, 2003. The right column (**B**, **D**, **F**) gives BaP concentrations (BaP, ng m^{-3}) with the ROI-T scheme and geopotential height (GH, m, contour lines) at different pressure level corresponding to figures in the left panel. Note that the brown and rose bold lines show the surface cold fronts and warm fronts, respectively.

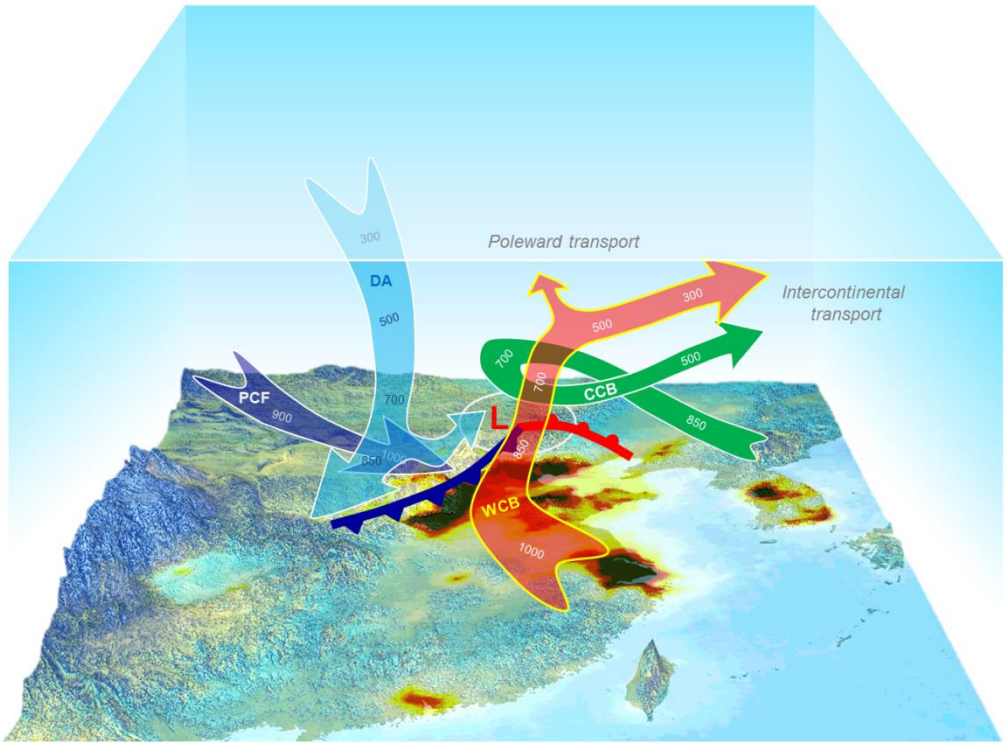

fig. S6. A conceptual scheme for air pollution transport due to middle-latitude cyclone. The warm conveyor belt (WCB) is the most efficient transport process for lifting air mass from boundary layer to middle- even upper- troposphere, which further contributes to intercontinental and poleward transport. Cold conveyor belt (CCB), dry air (DA) stream and post cold front (PCF) airstream contribute to the formation of WCB. The numbers marked on these belts indicate the pressure level (Figure modified with permissions from ref. *57*).